Simulation of ellipsometric spectra from nanocrystalline silicon floating gate structures

Kyung Hoon Jun, Seung Jae Baik, and Koeng Su Lim
Department of Electrical Engineering & Computer Science, Korea Advanced Institute of Science and Technology, 373-1 Guseong-dong, Yuseong-gu, Daejeon 305-701, Korea

Ho Seong Lee and Jeong Yong Lee
Department of Material Science and Engineering, Korea Advanced Institute of Science and Technology, 373-1 Guseong-dong, Yuseong-gu, Daejeon 305-701, Korea

(Received 10 December 2002; published 30 April 2003)

We simulated ellipsometric spectra from a nanocrystalline Si (nc-Si) floating gate structure: nc-Si grains embedded in a SiO_2 slab on crystalline Si substrate. An eigenmode analysis was carried out to incorporate light scattering effects in nc-Si. Geometric parameters were estimated by atomic force microscopy and transmission electron microscopy (TEM). Ellipsometry interpreted by the rigorous electromagnetic analysis removes the ambiguity in estimating the average size and the volume fraction of nanocrystals from TEM images. This work reveals that the scattering effect significantly modifies optical responses in a nanostructured semiconductor, whereas the effective medium theory cannot account for such an effect.

DOI: 10.1103/PhysRevB.67.155326 PACS number(s): 42.25.Fx, 78.20.Bh, 78.40.Fy, 78.67.Bf

I. INTRODUCTION

Recently a great deal of attention has been given to optical characterization of nanocrystalline materials[1,2] and the potentials of spectroscopic ellipsometry (SE) to the characterization of such materials are being increasingly explored.[3–6] SE is an attractive technique since it can nondestructively characterize the internal structure[5] and/or the dielectric function $(\varepsilon_1, \varepsilon_2)$.[6,7] The application of SE is moving from the well-established analysis of ideal layers to more complicated systems with nonideal effects.[8–11] In fact, light scattering effects in nanostructured semiconductors[12,13] have not been well studied for SE (Ref. 14) (or the reflection-and-transmission spectroscopy) in spite of the fact that such effects can play as artifacts for some sizes of morphologies. In order to address the problem and suggest a way to clarify it, we examined SE spectra of a nanocrystalline Si (nc-Si) floating gate structure:[15] nc-Si grains imbedded in a SiO_2 slab on crystalline Si (c-Si). For a rigorous interpretation, we simulated the spectra by the three-dimensional eigenmode formulation, in which the scattering process arising from the internal nanostructure can be incorporated. Due to the complexity of the electromagnetic problem in the SE analysis of nonideal structures, mathematical approaches have preceded to build correct physical interpretations.[8,16] The objective of this paper is to show the importance of scattering contribution in optical characterizations of nanostructured semiconductors. Up to date, the dielectric function of nanocrystal-containing layers have been taken as a mixture of ideal composites within the effective medium theory (EMT).[3–5] The EMT is valid when the length of the internal morphology is much smaller than the wavelength of the light internally propagating through the medium. Hujiwara *et al.* demonstrate a way to carefully treat the EMT in the valid wavelength range for SE study.[17] This paper will show that the EMT is not justifiable for the nanostructure since the scattering effect significantly modifies the ellipsometric response in a wide spectral range.

The nc-Si floating gate structure for memory devices receives a lot of attention due to the potentially high performance as well as the compatibility with general Si processes.[15,18,19] To manifest the scattering effect in nanocrystals, we have chosen rather a large grain size, in which a pronounced memory effect is still observed.[15,18] The structure considered in this paper can provide insights into the issue of light scattering effects in nanocrystals for several reasons. (i) The size distribution of nanocrystals in the nc-Si floating gate is relatively more uniform than in other bulklike nc-Si materials (e.g., porous silicon and silicon rich oxide) owing to the fact that the nc-Si floating gate possesses only a single nc-Si layer and the size becomes more uniform by self-limiting properties of oxidation process[20] adopted in this study. (ii) The nc-Si floating gate made by the deposition system used in this work has a fairly flat surface[21] otherwise, different scattering process can occur at the rough surface.[22–24] (iii) The thinness of the nc-Si layer allows us to obtain a relatively clear structural information near the interface with the substrate, otherwise the light carrying such information will be strongly absorbed by the nanocrystals. (iv) The thinness of the nc-Si layer also allows us to preclude the depolarization effect of light, which is the multiple scattering effect by randomly distributed scatterers.[14,25,26] (v) An incorporation of undesirable SiO_2, which changes the electronic structure of porous Si critically,[27,28] is not a problem here since SiO_2 is the isolator of nanocrystals.

II. EXPERIMENTS

We deposited nc-Si (nominally microcrystalline Si) film[29] by photochemical vapor deposition (photo-CVD).[30] Photo-CVD has advantages for ultrathin film application due to its low deposition rate and fine thickness controllability.[31] Air-oxidized p-type c-Si was used as substrate. Substrate temperature was 250 °C. The processing gas was a mixture of 1.3 sccm of SiH_4 and 19.6 sccm of H_2. Chamber pressure was kept at 0.55 Torr. Deposition time was 5 min. The as-

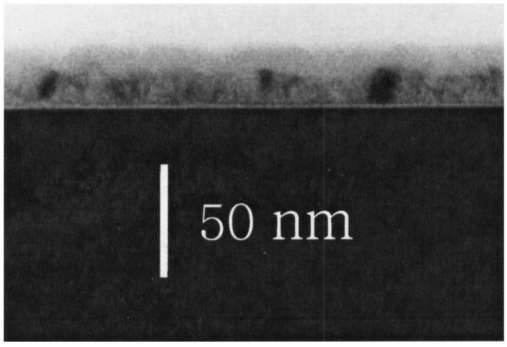

FIG. 1. XTEM image of the nc-Si floating gate.

deposited film was dehydrogenated in N_2 atmosphere at 430 °C for 1 h. Oxidation was performed at 900 °C for 30 min. Oxidation induces competing processes in a thin nc-Si film initially with amorphous Si matrix;[20] Si crystal growth and consumption of Si by oxidation. As oxidation proceeds, silicon film becomes thinner and eventually grains become split by SiO_2. At this situation, relatively large grains oxidize faster than smaller ones. We determined the root-mean-square (r.m.s.) roughness of the surfaces by atomic force microscopy (AFM). The AFM measurements were provided by the Autoprobe CP (PSIA corporation) in contact mode with scan window size of $1\times1\ \mu m^2$. The internal structure was observed by cross-section transmission electron microscopy (XTEM). The XTEM specimens were prepared by mechanical polishing followed by argon ion milling at liquid nitrogen temperature. A JEOL JEM 200EX microscope operating at 200 KV provided the XTEM micrographs. For the optical characterizations in the spectral range between 1.5 and 4.0 eV, we used a variable angle spectroscopic ellipsometer VUV-VASE (Woollam Co., Inc.).

III. MODELING OF nc-Si FLOATING GATE STRUCTURE

A precise optical description of the internal structure is needed not only to establish SE as a probe of nanostructures, but also to discuss light scattering effects in nanocrystals and eventually to deduce their true optical properties. In order to analyze SE spectra, we carefully estimated geometric parameters of the nc-Si floating gate from a number of XTEM images. Figure 1 displays a XTEM image of the nc-Si floating gate. The r.m.s. surface roughness is 1.25 nm by AFM. The thickness of the upper SiO_2 layer is around 11.6 nm $\pm$ 1.2 nm and that of the nc-Si layer is 12.5 nm $\pm$ 1.2 nm. The definition of average thickness values of the upper SiO_2 layer and the nc-Si layer faces an uncertainty due to an ambiguous brightness contrast in the XTEM image near the boundary between the two layers and due to the irregularity of the grain size. We will examine the effect of the thickness change in those two layers. The average distance between the grains seems to be the most difficult geometric parameter to define. The reason may be the nature of deposited nc-Si. The average distance between the grains will be discussed during the fitting procedure of geometric parameters. The thickness of the lower SiO_2 layer is 2.4 nm $\pm$ 0.2 nm.

We modeled the nc-Si floating gate as a two-dimensional multilayer grating. Figure 2 depicts the modeled structure. Region 1 represents surface roughness ($0<z<t_1$). We modeled region 1 as a layer having optical properties given by the Bruggeman type EMT as a 50%/50% mixture of SiO_2 and voids. Considering the small r.m.s. roughness of the surface measured by AFM, such an approximation is valid in the entire spectral range studied in this paper. Region 2 ($t_1<z<t_1+t_2$) represents the upper SiO_2 layer. Region 3 ($t_1+t_2<z<t_1+t_2+d$) represents the grating layer with nc-Si cubes of width d and the SiO_2 separator with thickness t_3. The period of the grating is h ($=d+t_3$) isotropically in x and y directions. Region 4 ($t_1+t_2+d<z<t_1+t_2+d+t_4$) represents the lower SiO_2 layer. Region 5 ($t_1+t_2+d+t_4<z$) is the c-Si substrate.

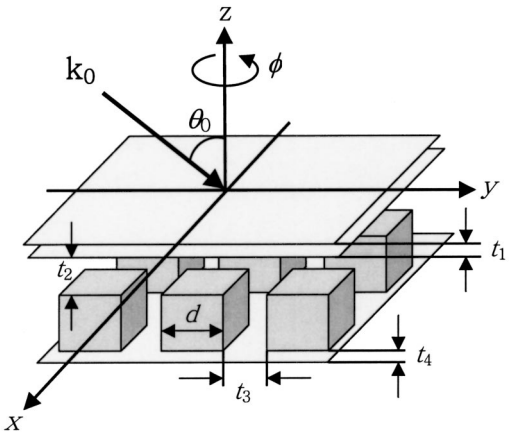

FIG. 2. The nc-Si floating gate structure modeled as a two-dimensional multilayer grating.

IV. COMPUTATIONAL METHOD

We applied the eigenmode theory[32,33] to simulate (Ψ, Δ) spectra from the nc-Si floating gate structure. Evaluation of eigenmode is widely used in the research fields of photonic crystals.[34,35] We used the geometric configuration shown in Fig. 2. Linearly polarized light (s and p polarization) of the wave vector $\mathbf{k}_0$ impinges on region 0 ($z<0$) with an incident angle of θ_0. The angle between $\mathbf{k}_0$ and the z axis is θ_0. For simplicity, the plane of incidence (defined by $\mathbf{k}_0$ and the z axis) is considered to contain the x axis, i.e., azimuthal angle ϕ_0 is 0°. The time dependence $\exp(-i\omega t)$ is assumed throughout this paper. Therefore the incident plane waves may be expressed in the form

$$\mathbf{E}_i(\mathbf{r}) = (\cos\theta_0\hat{\mathbf{x}} + \hat{\mathbf{y}} - \sin\theta_0\hat{\mathbf{z}})\exp(i\mathbf{k}_0\cdot\mathbf{r}), \tag{1}$$

where the incident wave vector can be expressed as

$$\mathbf{k}_0 = \alpha_0\hat{\mathbf{x}} + \gamma_0\hat{\mathbf{z}} = k_0\sin\theta_0\hat{\mathbf{x}} + k_0\cos\theta_0\hat{\mathbf{z}}, \tag{2}$$

where k_0 denotes the wave number in free space. The y component in Eq. (1) represents the s-polarized light and the other components represent p-polarized light. For simplicity, the magnitude of each polarization was normalized to unity. The reflected electric field in region 0 may be expressed as

$$\mathbf{E}_r(\mathbf{r}) = \sum_{m,n} \mathbf{R}_{m,n} \exp(i\mathbf{k}_{0mn} \cdot \mathbf{r}) \tag{3}$$

and the transmitted electric field in region 5 may be expressed as

$$\mathbf{E}_t(\mathbf{r}) = \sum_{m,n} \mathbf{T}_{m,n} \exp[i\mathbf{k}_{5mn} \cdot (\mathbf{r} - t_{\text{tot}}\hat{\mathbf{z}})], \tag{4}$$

where $t_{\text{tot}} = t_1 + t_2 + d + t_4$ and $\mathbf{R}_{mn}$ and $\mathbf{T}_{mn}$ represent the vector amplitudes of the reflected and the transmitted diffraction orders, respectively. The wave vectors of the diffraction orders in region 0 are

$$\mathbf{k}_{0mn} = \alpha_m \hat{\mathbf{x}} + \beta_n \hat{\mathbf{y}} - \gamma_{0mn} \hat{\mathbf{z}} \tag{5}$$

and in regions 1, 2, 4, and 5 are

$$\mathbf{k}_{jmn} = \alpha_m \hat{\mathbf{x}} + \beta_n \hat{\mathbf{y}} + \gamma_{jmn} \hat{\mathbf{z}}, \tag{6}$$

where $\alpha_m = \alpha_0 + 2\pi m/h$, $\beta_n = 2\pi n/h$, and

$$\gamma_{jmn} = \sqrt{k_j^2 - \alpha_m^2 - \beta_n^2}, \tag{7}$$

where k_j is the wave number in the jth region for all $j \neq 3$. The sign for region 0 and 5 are chosen so that the diffraction waves either propagate or decay away from the grating region.

The x component of the electric field in the regions 1, 2, 4 may be expressed as

$$E_{jx}(x,y,z) = \sum_{mn} \{A_{jmnx} \exp[i\gamma_{jmn}(z - t_{jup})] + B_{jmnx} \times \exp[-i\gamma_{jmn}(z - t_{jlo})]\} \exp[i(\alpha_m x + \beta_n y)], \tag{8}$$

where the subscript j defines the region, t_{jup} and t_{jlo} denote the upper and lower boundaries of the jth region, respectively. The coefficients A_{jmnx} and B_{jmnx} represent the amplitudes of the downward-going and the upward-going fields in the jth region, respectively. The y component of the electric field can be expressed in a similar way. The magnetic fields are obtained from the Maxwell's curl equation $\nabla \times \mathbf{E} = i\varpi\mu_0 \mathbf{H}$, where μ_0 is the magnetic permeability in free space (the media are assumed nonmagnetic).

The electric and magnetic fields in the modulated region 3 can be expressed in a pseudoperiodic Floquet form. Substituting the Floquet expressions of the electric and magnetic fields into the Maxwell's curl equations and writing the permittivity (i.e., dielectric function) distribution and its inverse as spatial Fourier expressions give the form of eigenvalue equations. If we take L orders both in the x and y directions, a numerical solution of the eigenvalue problem gives $2L^2$ eigenmodes that are identified by the propagation constants κ_l and the corresponding amplitudes E_{xmnl}, E_{ymnl}, H_{xmnl}, and H_{ymnl} ($l = 1,\ldots,2L^2$). The field in region 3 may be written as a superposition of the eigenmodes

$$E_{3x}(x,y,z) = \sum_{l=1}^{2L^2} \{A_{3l} \exp[i\kappa_l(z - t_{3up})] + B_{3l} \exp[-i\kappa_l(z - t_{3lo})]\} \times \sum_{m,n} E_{xmnl} \exp[i(\alpha_m x + \beta_n y)], \tag{9}$$

where t_{3up} and t_{3lo} denote the upper and lower boundaries of region 3, respectively, and the m and n summations extended over L^2 orders retained in the truncated Rayleigh series. The coefficients A_{3l} and B_{3l} represent the amplitudes of the downward-going and the upward-going fields in region 3, respectively. $E_{3y}(x,y,z)$, $H_{3x}(x,y,z)$, and $H_{3y}(x,y,z)$ can be expressed in a similar way.

The field coefficients can be determined by imposing the boundary conditions—tangential components of the electric and the magnetic fields should be continuous across the boundaries—accompanied by Maxwell's divergence equation $\nabla \cdot \varepsilon \mathbf{E}(\mathbf{r}) = 0$. The coefficients of the reflected field in the specular direction ($m = 0$ and $n = 0$) in Eq. (3) yields the ellipsometric angles (Ψ,Δ).

$$\rho = \frac{R_p}{R_s} = \tan\Psi e^{i\Delta}, \tag{10}$$

where, ρ is the complex amplitude reflection ratio, R_p is the reflection coefficient of the p-polarized light (x and z components), and R_s is the reflection coefficient of the s-polarized light (y component).

V. RESULTS AND DISCUSSION

In this section, we test the stability of our computation, choose geometric parameters to fit the simulated (Ψ,Δ) to the measured spectra, and compare the result from the eigenmode analysis with that from the EMT. During these procedures, we employed the dielectric function of thermally grown SiO_2 for the isolator and of polycrystalline Si (pc-Si) (Ref. 36) for the nanocrystals. These assumptions are based on the fact that a change of the electronic structure in the material induced by the quantum size effect can be ignored in this structure.[37]

To show the necessity of rigorous electromagnetic formulations, we consider $\sigma = |(2\pi/\lambda)\sqrt{\varepsilon_{\text{nc}}}d|$, where λ is the wavelength in free space and ε_{nc} is the dielectric function of the nanocrystals. If we set ε_{nc} to the values of pc-Si and $d = 13.7$ nm, σ varies from 0.39 for 1.5 eV to 1.67 for 4.0 eV. The σ values are beyond the Raleigh scattering regime ($\sigma \ll 1$), which implies the scattering can affect the SE spectra significantly for the structure studied in this paper.[38] The nonzero extinction coefficient values of TiO_2 nanocrystals at a lower energy than the bandgap energy in Ref. 3 was attributed to the presence of a scattering effect in the measurement, and the anomalous behavior of the dielectric function pointed out in Ref. 4 might be partly attributed to the inadequacy of the EMT approach.

Among a number of sets of the geometric parameters tested in the fitting procedure, we will exhibit some sets

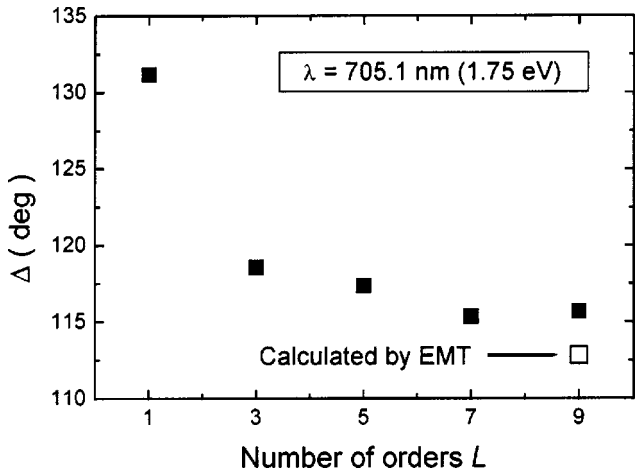

FIG. 3. Convergence of Δ as a function of the number of orders L. Data was collected at $E=1.65$ eV and $\theta_0=70°$. $t_1=1.25$ nm, $t_2=10.4$ nm, $d=13.7$ nm, $t_3=5.5$ nm, and $t_4=2.4$ nm. Δ simulated by the EMT with $f_c=25.1\%$ is also demonstrated.

showing the most distinguished tendencies. After determining the geometric parameters, we attempt to extract the dielectric function of the nc-Si, which may be different from the employed pc-Si values, by an inversion of the (Ψ,Δ) spectra.

Figure 3 shows convergence of Δ with respect to the number of orders L retained along each direction. Data was collected at $E=1.65$ eV and $\theta_0=70°$. The geometric parameters were $t_1=1.25$ nm, $t_2=10.4$ nm, $d=13.7$ nm, $t_3=5.5$ nm, and $t_4=2.4$ nm. For comparison, Δ simulated by the Bruggeman type EMT is demonstrated in Fig. 3. The displayed crystalline volume fraction, f_c (=25.1%) was determined by $d^3/h^2 t_{\mathrm{tot}}$. For the EMT calculation, we used a four-layer stack (air/mixture of voids and SiO_2/mixture of pc-Si and SiO_2/c-Si substrate) model. The thickness for the surface was t_1 and for the bulk layer was set to t_2+d+t_4 $(=t_{\mathrm{tot}}-t_1)$. The presence of many evanescent modes increases the computational complexity. The high ε_2 at the nc-Si layer restricts the convergence of the numerical implementation by enhancing the evanescent modes. With the geometric parameters for the result in Fig. 3, the calculation becomes unstable for $L>9$. Fortunately, as one can see from Fig. 3, the convergence is quite satisfactory when we truncated the number of orders at $L=7$. We should note that the converged value by a moderate truncation in the eigenmode analysis is evidently different from the result calculated by the EMT.

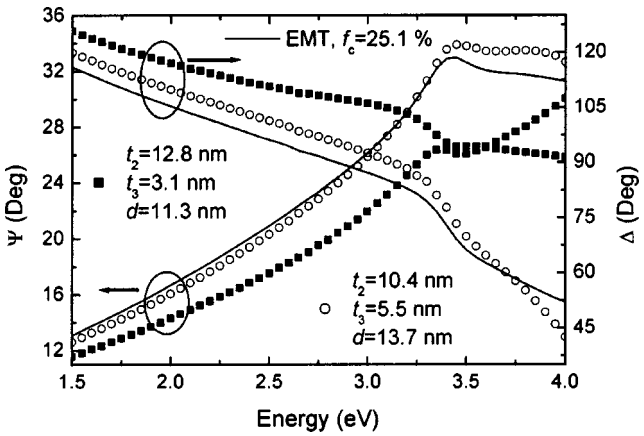

FIG. 4. (Ψ,Δ) at different geometric parameters associated with the same f_c(=25.1%). Data was collected at $\theta_0=70°$. t_1 and t_4 were fixed at 1.25 and 2.4 nm, respectively. (Ψ,Δ) simulated by the EMT with $f_c=25.1\%$ are also displayed.

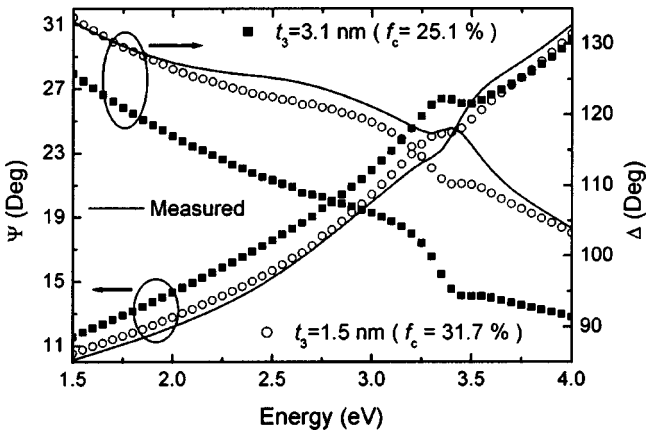

FIG. 5. (Ψ,Δ) at different t_3. Data was collected at $\theta_0=70°$. $t_1=1.25$ nm, $t_2=10.4$ nm, $d=13.7$ nm, and $t_4=2.4$ nm. The corresponding f_c are 25.1% for $t_3=5.5$ nm and 31.7% for $t_3=1.5$ nm. Measured (Ψ,Δ) are also displayed.

Figure 4 displays (Ψ,Δ) at different geometric parameters associated with the same f_c (=25.1%). Data was collected at $\theta_0=70°$. t_1 and t_4 were fixed at 1.25 and 2.4 nm, respectively. We truncated the number of orders L to satisfy both the convergence and the numerical stability. For the structure of $t_1=1.25$ nm, $t_2=10.4$ nm, $d=13.7$ nm, $t_3=5.5$ nm, and $t_4=2.4$ nm, we took $L=7$, and for the other structure $L=5$. The (Ψ,Δ) simulated by the EMT with $f_c=25.1\%$ is displayed for comparison. The procedure for EMT calculation is the same as with Fig. 3. Generally, it is difficult to estimate the average value of all the geometric parameters accurately from the difference of diffraction contrasts in XTEM images. Figure 4 considers two extremities for the average size of nanocrystals d that can be deduced from XTEM images of the same nc-Si floating gate samples. When the structure has the same f_c, the discrepancy in the

air		
surface roughness		0 nm
upper SiO_2		13.7 nm
mixture by EMT	pc-Si 83.6 % SiO_2 16.4 %	19.0 nm
lower SiO_2		0.6 nm
c-Si substrate		

FIG. 6. Schematic layer profiles of nc-Si floating gate fitted by the six-layer stack model employing the EMT for the surface roughness and the nc-Si layer.

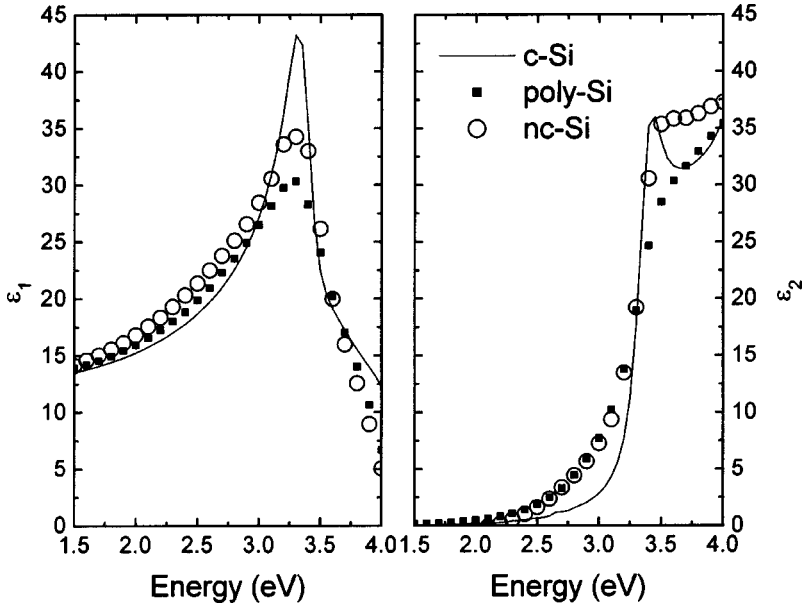

FIG. 7. Extracted $(\varepsilon_1,\varepsilon_2)$ of the nc-Si. For the fitting procedure, the simulation was carried out with the geometric parameters of $t_1=1.25$ nm, $t_2=12.8$ nm, $d=11.3$ nm, $t_3=1.5$ nm, and $t_4=2.4$ nm, and the data was collected at $\theta_0=70°$. $(\varepsilon_1,\varepsilon_2)$ of the *c*-Si and the pc-Si are also displayed.

simulated (Ψ,Δ) between the eigenmode analysis and the EMT is larger for smaller *d*. The measured spectra will prove that the eigenmode simulation with the smaller *d* is closer to the reality.

Figure 5 depicts (Ψ,Δ) at different t_3. Data was collected at $\theta_0=70°$. The other geometric parameters were fixed at $t_1=1.25$ nm, $t_2=10.4$ nm, $d=13.7$ nm, and $t_4=2.4$ nm. We took $L=7$. As t_3 decreases from 5.5 to 1.5 nm, the corresponding f_c increases from 25.1 to 31.7%. The simulated (Ψ,Δ) spectra from the structure with $t_3=1.5$ nm fit moderately with the measured values. This geometric parameter set gives the best fit so far. The rest of the difference between the measured and the simulated values will be attributed to the difference of the $(\varepsilon_1,\varepsilon_2)$ between the pc-Si and the nc-Si. It will be discussed further below.

We have noticed from Figs. 3 and 4 that the (Ψ,Δ) spectra simulated by the EMT deviates much from the values obtained by the rigorous electromagnetic analysis. To explore the possibility of finding the true geometric parameters by ignoring the scattering contribution from nanocrystals, we determined them by an extensive fitting procedure using a six-layer stack (air/mixture of voids and SiO_2/upper SiO_2/mixture of pc-Si and SiO_2/lower SiO_2/*c*-Si substrate) model adopting the Bruggeman type EMT for the mixture layers. We fixed the volume fraction as 50%/50% for voids and SiO_2 in the surface layer. We varied the thickness for all layers and the f_c for the nc-Si layer freely to yield the best fit of the simulated (Ψ,Δ) to the measured spectra. Figure 6 illustrates the determined geometric parameters. The thickness values from this approach are far from even a rough estimation by the XTEM image shown in Fig. 1. This implies that the optical simulation ignoring scattering effects in nanocrystals is apt to render an unrealistic interpretation.

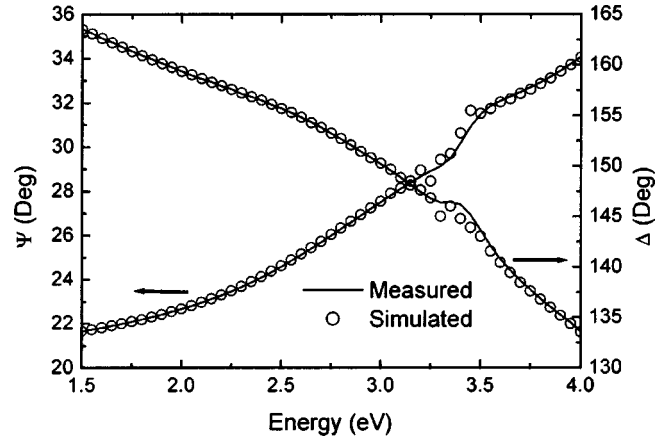

FIG. 8. Measured and simulated (Ψ,Δ) collected at $\theta_0=60°$. The deduced $(\varepsilon_1,\varepsilon_2)$ of the nc-Si in Fig. 7 and the geometric parameters for the determination of the $(\varepsilon_1,\varepsilon_2)$ were used for the simulation.

As the size of nc-Si decreases significantly, its dielectric function starts to differ from the bulk state according to the change of electronic structure. Spatial confinement in low-dimensional nanostructures causes the relaxation of the wave vector *k*-selection rule, widens the bandgap, and enhances the oscillator strength in the lowest optical transition regime. Whereas there are a number of theoretical studies of the optical properties of the nanostructured silicon,[1,37] little experimental work has been done to demonstrate its dielectric function in a wide spectral range. We deduced the $(\varepsilon_1,\varepsilon_2)$ by mathematical inversion of the (Ψ,Δ) spectra in view of the possibility to provide $(\varepsilon_1,\varepsilon_2)$ spectra of such a nanostructured semiconductor by SE. Figure 7 shows the deduced $(\varepsilon_1,\varepsilon_2)$ of the nc-Si with the geometric parameters of $t_1=1.25$ nm, $t_2=12.8$ nm, $d=11.3$ nm, $t_3=1.5$ nm, and $t_4=2.4$ nm. Both the measured and simulated data were collected at $\theta_0=70°$. For comparison, $(\varepsilon_1,\varepsilon_2)$ of the *c*-Si and the pc-Si are displayed. A major hindrance toward establishing such an interpretation is the lack of comparable data, which relate the size of nc-Si to $(\varepsilon_1,\varepsilon_2)$ spectra. As a second method to check the reliability of the deduced values, we demonstrate in Fig. 8, a comparison of the measured and simulated (Ψ,Δ) spectra collected at $\theta_0=60°$, using the

$(\varepsilon_1,\varepsilon_2)$ deduced by the previous procedure. If the set of determined geometric parameters and $(\varepsilon_1,\varepsilon_2)$ from the fitting procedure collected at $\theta_0=70°$ is far from reality, it will lead to the discrepancy between the simulated and measured values collected at $\theta_0=60°$. As Fig. 8 exhibits, the simulation fits moderately with the measured spectra in the entire displayed range. The simulation at $\theta_0=60°$ shows a certain disagreement with the measured values near 3.3 eV. We believe that this behavior originates from a numerical instability due to the high $(\varepsilon_1,\varepsilon_2)$ values near that point.

The $(\varepsilon_1,\varepsilon_2)$ spectra of the nc-Si in Fig. 7 generally follow the tendency of the pc-Si, where critical point broadening[40] and light absorption enhancement in the energy range of indirect transition[26] are observed. These effects are known to be irrelevant with quantum confinement effects and the reasons are treated elsewhere.[41,42] On the other hand, two mentionable features in Fig. 7 are (i) ε_1 of the nc-Si is even higher than pc-Si in the indirect transition range and (ii) the critical point of the nc-Si, in which the first direct transition occurs, shows less broadened peaks than pc-Si. In our opinion, the first feature can be attributed to the slightly elevated oscillator strength even if a distinctive elevation must occur in smaller sizes of nanocrystals.[37,39] The critical point broadening effect in the second feature is generally attributed to a reduction in the excited-state lifetime of electrons due to scattering from grain boundaries or defects. The second feature suggests a lower defect density of the nc-Si than the compared pc-Si, based on the fact that a smaller nc-Si than the pc-Si would show the opposite tendency since the nc-Si has more grain boundaries in a unit volume. The peculiar memory effect of its device shown in Ref. 15 also suggests the low defect density in the nc-Si. It is possible that the defect density in the nc-Si is reduced when the sample was fabricated through the annealing and the oxidation procedure. Apart from the mentioned features, a change of the bandgap in the nc-Si seems difficult to discuss in this work since ε_2 becomes slightly lower than 0 towards lower energy in $E<2.15$ eV and reaches -0.788 at $E=1.5$ eV. We have observed that the optical absorption coefficient (not shown in this paper) of the nc-Si shows rather sharp transition compared to pc-Si near the onset of indirect transition. An extraction of the true dielectric function of the embedded nc-Si from a pseudodielectric function by this approach requires a highly accurate description of the structure. The eigenmode approach employed in this paper does not consider irregularities of the size, position, and shape of nanocrystals. Errors might have occurred in investigating into the geometric parameters together with the limitation in the ideal model. Cogent discussions on $(\varepsilon_1,\varepsilon_2)$ spectra of nc-Si are left until a more precise estimation of the accuracy in the simulation is available.

VI. CONCLUSIONS

We have simulated SE spectra of the nc-Si floating gate structure by the eigenmode analysis. Geometric parameters were estimated by AFM and XTEM and the SE study clarified the ambiguity in those estimations. In contrast to the EMT approach, the eigenmode analysis is proven to account for light scattering effects in the nanostructure.

One who aims to discuss the electronic structure of nanocrystalline semiconductors by optical measurements has to be careful in discriminating the scattering contribution and the intrinsic property of the material in the measured spectra. We believe that our interpretation of SE spectra of the nc-Si floating gate structure gives a meaningful implication in understanding of the light scattering effects in nanocrystals. None of the previous optical characterizations seems to have quantitatively discussed such effects. This approach may be successfully applied to explore the optical properties of various nanocrystal assemblies.

ACKNOWLEDGMENTS

The authors are grateful to Y. J. Cho and S. H. Kim in Korea Research Institute of Standards and Science for the support of SE measurements, to J. Y. Ahn and T. H. Kim for the sample preparation, and to O. Chevaleevski, O. P. Agnihotri, and H. J. Eom for the helpful discussions. This work was supported by the Brain Korea 21 project in 2002.

[1] I. Vasiliev, S. Öğüt, and J. R. Chelikowsky, Phys. Rev. Lett. **86**, 1813 (2001).
[2] T. Matsumoto, J. Suzuki, M. Ohnuma, Y. Kanemitsu, and Y. Masumoto, Phys. Rev. B **63**, 195322 (2001).
[3] Md. Mosaddeq-ur-Rahman, G. Yu, T. Soga, T. Jimbo, H. Ebisu, and M. Umeno, J. Appl. Phys. **88**, 4634 (2000).
[4] R. Serna, J. C. G. de Sande, J. M. Ballesteros, and C. N. Afonso, J. Appl. Phys. **84**, 4509 (1998).
[5] M. Losurdo, G. Bruno, D. Barreca, and E. Tondello, Appl. Phys. Lett. **77**, 1129 (2000).
[6] H. V. Nguyen, Y. Lu. S. Kim, M. Wakagi, and R. W. Collins, Phys. Rev. Lett. **74**, 3880 (1995).
[7] S. Adachi and H. Mori, Phys. Rev. B **62**, 10 158 (2000).
[8] M. Schubert, Phys. Rev. B **53**, 4265 (1996).
[9] G. E. Jellison, Jr. and L. A. Boatner, Phys. Rev. B **58**, 3586 (1998).
[10] U. Rossow, Thin Solid Films **313–314**, 97 (1998).
[11] M. Forcht, A. Gombert, R. Joerger, and M. Köhl, Thin Solid Films **313–314**, 808 (1998).
[12] S. M. Scholz, R. Vacassy, J. Dutta, and H. Hofmann, J. Appl. Phys. **83**, 7860 (1998).
[13] P. Ferrand and R. Romestain, Appl. Phys. Lett. **77**, 3535 (2000).
[14] K. H. Jun and K. S. Lim, Appl. Opt. **42**, 1211 (2003).
[15] S. J. Baik, J. H. Choi, J. Y. Lee, and K. S. Lim, Superlattices Microstruct. **28**, 477 (2000).
[16] D. E. Aspnes, Phys. Rev. B **41**, 10 334 (1990).
[17] H. Fujiwara, J. Koh, P. I. Rovira, and R. W. Collins, Phys. Rev. B **61**, 10 832 (2000).
[18] S. J. Baik and K. S. Lim, Appl. Phys. Lett. **81**, 5186 (2002).
[19] S. Tiwari, F. Rana, H. Hanafi, A. Hartstein, E. F. Crabbé, and K.

Chan, Appl. Phys. Lett. **68**, 1377 (1996).
[20] H. I. Liu, D. K. Biegelsen, F. A. Ponce, N. M. Johnson, and R. F. W. Pease, Appl. Phys. Lett. **64**, 1383 (1994).
[21] K. H. Jun, K. S. Lim, S. Y. Kim, and S. J. Kim, J. Non-Cryst. Solids **275**, 59 (2000).
[22] S. Krishnan and P. C. Nordine, Appl. Opt. **33**, 4184 (1994).
[23] K. H. Jun, J. H. Kwak, and K. S. Lim, J. Opt. Soc. Am. A (to be published in June 2003).
[24] R. M. A. Azzam and N. M. Bashara, Phys. Rev. B **5**, 4721 (1972).
[25] K. Forcht, A. Gombert, R. Joerger, and M. Köhl, Thin Solid Films **302**, 43 (1997).
[26] K. H. Jun, H. Stiebig, and R. Carius, Phys. Rev. B **66**, 115301 (2002).
[27] U. Frotscher, U. Rossow, M. Ebert, C. Pietryga, W. Richter, M. G. Berger, R. Arens-Fischer, and H. Münder, Thin Solid Films **276**, 36 (1996).
[28] I. Vasiliev, J. R. Chelikowasky, and R. M. Martin, Phys. Rev. B **65**, 121302(R) (2002).
[29] E. Edelberg, S. Bergh, R. Naone, M. Hall, and E. S. Aydil, J. Appl. Phys. **81**, 2410 (1997).
[30] J. H. Jang and K. S. Lim, Jpn. J. Appl. Phys. **35**, 5625 (1996).
[31] K. H. Jun and K. S. Lim, J. Non-Cryst. Solids **261**, 268 (2000).
[32] M. Jiang, T. Tamir, and S. Zhang, J. Opt. Soc. Am. A **18**, 807 (2001).
[33] E. Noponen and J. Turunen, J. Opt. Soc. Am. A **11**, 2494 (1994).
[34] V. Kuzmiak and A. A. Maradudin, Phys. Rev. B **58**, 7230 (1998).
[35] S. G. Tikhodeev, A. L. Yablonskii, E. A. Muljarov, N. A. Gippius, and T. Ishihara, Phys. Rev. B **66**, 045102 (2002).
[36] G. E. Jellison, Jr. and M. F. Chisholm, and S. M. Gorbatkin, Appl. Phys. Lett. **62**, 3348 (1993).
[37] B. Delley and E. F. Steigmeier, Phys. Rev. B **47**, 1397 (1993).
[38] J. A. Stratton, in *Electromagnetic Theory* (McGraw-Hill, New York, 1941), p. 570.
[39] P. E. Batson and J. R. Heath, Phys. Rev. Lett. **71**, 911 (1993).
[40] G. E. Jellison, Jr. and M. F. Chisholm, and S. M. Gorbatkin, Appl. Phys. Lett. **62**, 3348 (1993).
[41] G. E. Jellison, Jr., S. P. Withrow, J. W. McCamy, J. D. Budai, D. Lubben, and M. J. Godbole, Phys. Rev. B **52**, 14 607 (1995).
[42] L. Viña and M. Cardona, Phys. Rev. B **29**, 6739 (1984).